Striated organelle, a cytoskeletal structure positioned to modulate hair-cell transduction

Florin Vranceanu[a], Guy A. Perkins[b], Masako Terada[b], Robstein L. Chidavaenzi[a], Mark H. Ellisman[b], and Anna Lysakowski[a,1]

[a]Department of Anatomy and Cell Biology, University of Illinois, Chicago, IL 60612; and [b]National Center for Microscopy and Imaging Research, Center for Research in Biological Systems, University of California at San Diego, La Jolla, CA 92093

Edited by Bechara Kachar, National Institutes of Health, Bethesda, MD, and accepted by the Editorial Board January 30, 2012 (received for review January 19, 2011)

The striated organelle (SO), a cytoskeletal structure located in the apical region of cochlear and vestibular hair cells, consists of alternating, cross-linked, thick and thin filamentous bundles. In the vestibular periphery, the SO is well developed in both type I and type II hair cells. We studied the 3D structure of the SO with intermediate-voltage electron microscopy and electron microscope tomography. We also used antibodies to α-2 spectrin, one protein component, to trace development of the SO in vestibular hair cells over the first postnatal week. In type I cells, the SO forms an inverted open-ended cone attached to the cell membrane along both its upper and lower circumferences and separated from the cuticular plate by a dense cluster of exceptionally large mitochondria. In addition to contacts with the membrane and adjacent mitochondria, the SO is connected both directly and indirectly, via microtubules, to some stereociliary rootlets. The overall architecture of the apical region in type I hair cells—a striated structure restricting a cluster of large mitochondria between its filaments, the cuticular plate, and plasma membrane—suggests that the SO might serve two functions: to maintain hair-cell shape and to alter transduction by changing the geometry and mechanical properties of hair bundles.

actin | cytoskeleton | stereocilia | ultrastructure | sensory receptors

Hair-cell stereocilia are important for mechanotransduction. Much is known about their structure, their mechanical properties, and their geometric arrangement (1–3). These cells are embedded in the cuticular plate, a dense structure composed of an actin gel (4) located at the apical end of the hair cell, which is thought to act as a rigid platform, helping stereocilia return to their resting positions after stimulus-evoked displacements (5, 6). What has never been investigated is how the cuticular plate might be stabilized by structures underneath it. Do these structures provide a foundation for the cuticular plate and the hair bundle?

One such structure is the striated organelle (SO), also known as a laminated (or Friedman's) body, which is a cytoskeletal lattice underlying the apicolateral hair-cell membrane and consisting of alternating thick and thin filament bundles. When first described in vestibular hair cells in the 1960s, this structure was thought to be a pathological feature (7, 8). It was later found to be a normal component of mammalian vestibular and cochlear inner, but not outer, hair cells (9–11). A striated structure, similar in position but differing in morphological details, has been described in other vertebrates (12–14).

Slepecky et al. provided a description of the SO (10, 15, 16), including the periodicity of its filaments, their radial direction, attachment to the plasma membrane, and association with microtubules. Previous studies, even those based on conventional transmission electron microscopy (TEM) and deep-etch freeze fracture (9, 10, 15, 17, 18), did not provide a picture of the 3D structure of the organelle. Electron-microscopic tomography (EMT) provides a promising approach to study 3D structures. The approach has been used to study other structural features of hair cells (19, 20) and is used here to study the SO's 3D architecture, localization, shape, size, prevalence, and its connections with neighboring structures. We also used immunochemistry to identify and localize one protein component and to trace the development of the SO over the first postnatal week.

Our findings on SO structure and 3D architecture of the apical region in vestibular hair cells reveal previously undescribed aspects of hair-cell cytoskeletal organization and suggest new hypotheses about the hair bundle and mechanoelectric transduction.

Results

Material was examined with both conventional TEM and intermediate voltage electron microscopy (IVEM, 400 KeV). Results were similar in both cases. From these data and EMT software, we produced 3D reconstructions of the SO and the apical portion of three type I hair cells (cells 1–3) and one type II cell (cell 4) from the utricular macula. Extrastriolar hair cells were preferred because they are smaller than those from the striola, which allowed us to use a magnification high enough (5,000×) to see details, but low enough to get the whole apical hair cell in the field of view. Three reconstructions (cells 1, 3, and 4) were partial, and the other (cell 2) encompassed the entire apical portion of the hair cell. We also obtained tomographic data, but no reconstructions, from one striolar type I cell (cell 5) and a second type II cell (cell 6). In each reconstruction, we modeled the thick and thin filament bundles of the SO, the stereociliar rootlets (SRs), the cuticular plate, subcuticular mitochondria, and the membranes of the hair cell and surrounding calyx (the afferent ending innervating a type I hair cell) to obtain a 3D model of the SO in relation to these other structures.

Structure of the SO. Each SO was composed of 35–40 thick bundles of filaments and an equal number of thin bundles (Fig. 1*A*). These bundles had thicknesses of 34.6 ± 1.25 nm (mean ± SD), $n = 59$, and 11.3 ± 0.45 nm, $n = 54$, respectively. Individual filaments within the thick and thin bundles measured ∼10 nm and 6 nm, respectively. Thick bundles were located immediately subjacent to the cell membrane (Fig. 1 *A* and *B*), and exhibited a periodicity of 128 ± 3.1 nm ($n = 56$); thin bundles were located midway between adjacent thick ones. The bundles of intertwined filaments (Fig. 1*A*, *Inset*) extended radially, like spokes, from the plasma membrane ∼130 nm into the hair cell (Fig. 1*B*). Along the length of the organelle, bundles could be oriented vertically (Figs. 1*A* and 2 *A* and *B*) or spirally (Figs. 1 *E* and *F* and 2*F*). Sometimes both orientations were found in restricted regions of a single organelle.

In type I hair cells, several bundles extended upwards from their circumferential location below the cuticular plate and inserted into the apical membrane surrounding the kinocilium

Author contributions: F.V., R.L.C., and A.L. designed research; F.V., G.A.P., R.L.C., and A.L. performed research; M.H.E. contributed new reagents/analytic tools; F.V., G.A.P., M.T., R.L.C., and A.L. analyzed data; and F.V. and A.L. wrote the paper.

The authors declare no conflict of interest.

This article is a PNAS Direct Submission. B.K. is a guest editor invited by the Editorial Board.

Freely available online through the PNAS open access option.

[1]To whom correspondence should be addressed. E-mail: alysakow@uic.edu.

This article contains supporting information online at www.pnas.org/lookup/suppl/doi:10.1073/pnas.1101003109/-/DCSupplemental.

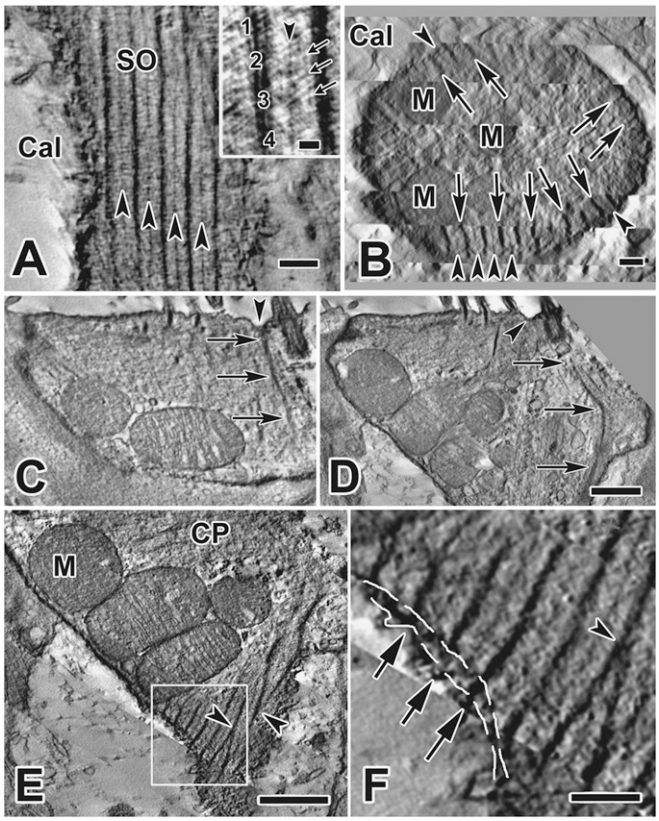

Fig. 1. Structure of the SO. (*A*) Tangential section from a type I hair cell EM tomogram showing the structure, periodicity, and location of the SO immediately subjacent to the calyx membrane. (*Inset*) Thick (numbered) and thin (arrowhead*)* filament bundles are composed of several thinner, spiral-bundled filaments (e.g., 1–4), measuring ~10 nm and ~6 nm, respectively. Note also the cross filaments (small arrows), which EM immunogold studies indicate are likely spectrin (Fig. 5 *B* and *C*, and *Insets*). (Scale bar, 0.2 μm.) (*B*) Cross-section through the neck of a type I cell showing radial distribution of thick (arrows) and thin (arrowheads) SO filament bundles. They extend from the hair cell membrane to a depth of ~130 nm into the cell. (Scale bar, 0.2 μm.) (*C* and *D*) Apical insertion of a thick SO filament bundle (arrows) adjacent to the kinocilium. The site of insertion is a dimpled area (arrowhead) between the kinocilium and nearby SRs. (*D*) A SO filament bundle angles downward (arrows), approaching the cell membrane and continuing into the neck of the type I cell. (Scale bar, 0.5 μm; also applies to *C*.) (*E* and *F*) Details of hair-cell neck region in cell 2, obtained with SLICER mode in IMOD. (*E*) Thick filament bundles of the SO merge together (arrowheads). (Scale bar, 1 μm.) (*F*) Higher magnification of the area enclosed in the box in *E* shows possible connections (arrows) between thick filament bundles of the SO and the calyx membrane bridging the intercellular cleft (dashed white lines show locations of hair-cell and calyx membranes). (Scale bar, 0.25 μm.). Cal, calyx; CP, cuticular plate; M, mitochondria.

(Fig. 1 *C* and *D*); the point of insertion is dimpled, as if the bundle were exerting a pulling force on the apical membrane. Within the SO, thick bundles often merged with one another (Fig. 1*E*) or morphed into thin bundles. Some bundles even appeared to cross the intercellular cleft between the hair cell and the calyx ending and insert into the calyx membrane (Fig. 1 *E* and *F*). Overall, the SO is shaped like an inverted conical cage (Fig. 2 and Movies S1 and S2), with the upper, larger opening facing the cuticular plate.

Connections of the SO to the Kinocilium and Some Stereocilia. The linkage between the membrane surrounding the kinocilium and the SO was seen in several cells. On occasion, SO bundles were observed to connect to SRs. This link was seen in a tomogram section for cell 1 (Fig. 2*A*) and in the resulting model (Fig. 2*B*). Two neighboring SRs merged, seemingly without interruption, into separate SO thick bundles. A similar observation was made in serial TEM photos (Fig. S1). In both instances, the SRs continuous with SO filaments were located on the circumference of the hair bundle. The SRs were slightly thicker than their continuations with the SO (Fig. 2*A*), suggesting that the two elements may differ in protein composition, or that, if both are made up of the same proteins, the latter is bundled differently.

Stereociliar Rootlets. We measured the diameters of stereocilia and SRs across all rows of the hair bundle in two hair cells. Stereocilia nearest the kinocilium (rows 1–3), were significantly thicker than those in rows 4–10 (stereocilia: rows 1–3, 140.6 ± 3.5, $n = 34$ vs. rows 4–10, 116.0 ± 3.4, $n = 114$, $P < 0.05$; rootlets: 46.1 ± 1.7, $n = 34$ vs. 38.0 ± 1.9, $n = 114$, $P < 0.05$). In all type I hair cell reconstructions, the largest SRs, those nearest the kinocilium, bent to form an angle of 110° within the cuticular plate (cell 2) (Fig. 2*C* and Movie S2). A type I cell from the striolar region (Fig. 2*C*, *Inset*), oriented in an appropriate plane, showed several rootlets bending within the cuticular plate. These long rootlets, on passing through the cuticular plate (Fig. 2*C*, *Inset*), were organized into two groups (Fig. 2*E*) that converged toward separate areas on the hair-cell membrane opposite the kinocilium (the SR insertion area) (Fig. 2*D*). The arrangement is best seen by observing the SR insertion area from different angles, as in the movie (Movie S2). SRs further from the kinocilium exhibited less and less bending and most appeared to remain within the cuticular plate (Fig. 2*F* and Movie S2).

Subcuticular Mitochondria. Within the confines of the SO, there is a set of exceptionally large mitochondria compared with those in the rest of the type I cell or in type II cells. Because mitochondrial function (Ca^{2+} homeostasis and source of ATP) is related to overall size, we used our tomograms to measure the volumes and surface areas of mitochondria from the same portion of the cell (the subcuticular region, ~6 μm below the apical cell membrane) in type I and neighboring type II cells (Table S1). Table S1 indicates that mitochondria inside the SO in type I hair cells are two-times larger in surface area and three- to four-times larger in volume than those in type II cells. In one reconstruction (cell 1), a few SRs emerging from the underside of the cuticular plate ended on subcuticular mitochondria and appeared to be "tethered" to them (Fig. 3 *A* and *B*). In cell 2, other mitochondria were intimately associated with long stretches of SO bundles (Fig. 3 *C* and *D*). We observed similar close associations in each of the other reconstructions: for example, cell 4 (Fig. 4*D*).

SO in Vestibular Type II Hair Cells. EMT results from the partial reconstruction of a type II cell (cell 4) are shown in Fig. 4. The SO is more extensive in the type II hair cell than in type I cells. It is longer, broader in extent, and the thick bundles are wider (compare Figs. 4 *A–C* and 5*A*) and can extend deeper into the hair cell (~400 nm, compared with ~130 nm for type I hair cells). Spherical structures surround the SO and are more numerous than in type I cells. Merging and morphing filaments were observed. Viewing the model from a vantage point below the cuticular plate (Fig. 4*D*), we can see that the SO is not connected to stereocilia in this cell, but it is closely associated with four mitochondria along its breadth, similar to type I cells (Fig. 3 *C* and *D*).

Protein Composition of the SO. We have identified one protein in the SO (Fig. 5). Using an antibody to α-2 spectrin, we labeled the SO in vestibular hair cells in both confocal (Fig. 5*A*) and EM immunogold (Fig. 5 *B* and *C*) experiments. Quantification of the EM label for α-2 spectrin indicated a nonhomogeneous distribution of gold particles, with a tendency for them to be located immediately adjacent to the thick filament bundles (Fig. 5*C*) (χ^2 test of homogeneity, $\chi^2 = 23.1$, $df = 7$, $P < 0.002$). Western blots (Fig. S2*A*) confirmed the presence of α-2 spectrin in the inner ear. The identities of the bands at 150 kD and 285 kD were confirmed as α-2 spectrin with mass spectrometry (Fig. S2*B*).

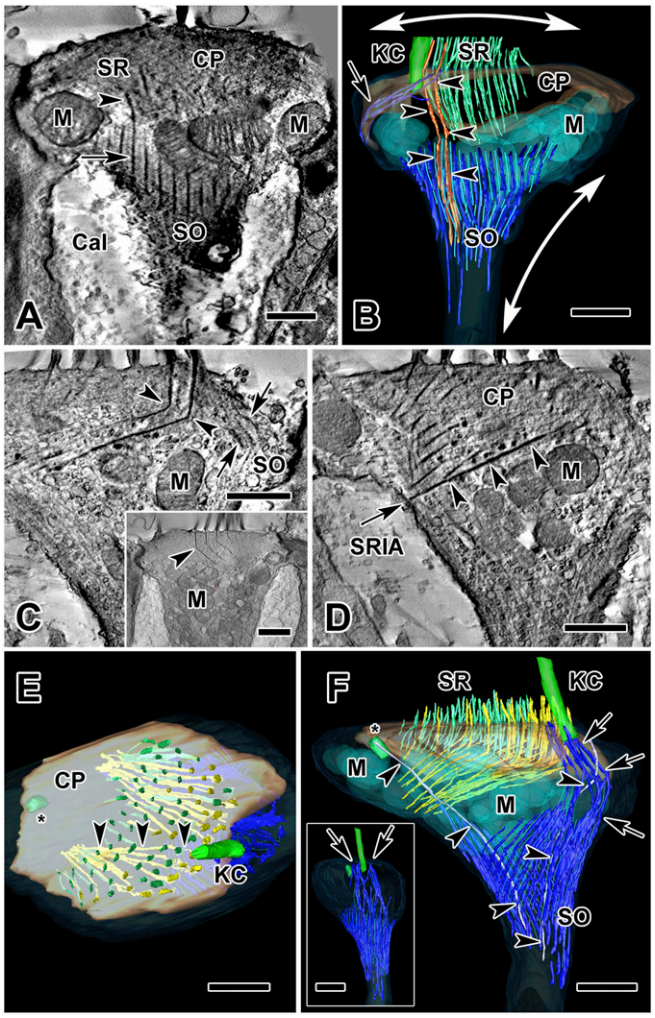

Fig. 2. Tomograms and reconstructions of two type I hair cells. (*A*) Tomogram section of cell 1, a juxtastriolar type I cell, showing the connection between a SR (arrowhead) and a SO thick filament bundle (arrow). (*B*) Three-dimensional reconstruction of the same type I hair cell from a volume obtained by joining six serial tomograms (3.0 μm total thickness). The apical part of the SO extends from the lateral aspect of the cell membrane (arrow) to the apical hair cell membrane near the kinocilium. Two SRs are continuous with the SO (orange, arrowheads). SO thick (dark blue) and thin (light blue) filament bundles envelop a group of large mitochondria (transparent light blue). One possible effect on cell shape and hair bundle tension, based on filament direction and cell membrane insertions is illustrated: radial contraction of the SO elongates the neck of the hair cell (vertical two-headed arrow), which simultaneously splays the hair bundle through the connection of the rootlets with the SO (horizontal two-headed arrow). (*C–F*) Cell 2, an extrastriolar type I cell, modeled by joining 11 serial tomograms (total volume thickness = 5.5 μm). (*C*) One section from this tomogram shows a 110° bend in two of the longest rootlets (arrowheads). An apical extension of the SO (arrows) near the kinocilium (not seen in this section), is also shown in the model (see below, *F* and *F Inset*, arrows). (*Inset*) Section from cell 5, a striolar type I hair cell, fortuitously illustrating four bent rootlets in a single plane. (*D*) The lower of two SRs in *C* (arrowheads) traverses the cuticular plate and inserts into the SR insertion area (arrow) on the cell membrane on the opposite side of the cell. (*E*) A view from the top of the hair cell in *C* and *D*. Inside the cuticular plate, long, bent SRs (yellow, arrowheads), originating near the kinocilium and identical to those in *C* and *D*, traverse the cuticular plate and insert in the plasma membrane; thinner, green stereocilia (located farther from the kinocilium) do not traverse the cuticular plate. (*F*) Lateral view of the 3D model of cell 2. Thick (dark blue) and thin (light blue) SO filament bundles are distinguished. Arrows point to an extension of the SO that encircles the kinocilium. Nearby, a kinociliar rootlet (gray, arrowheads) extends from the kinocilium down toward the neck of the hair cell; another (arrowheads) is observed extending from the centriole (asterisk). (*Inset*) Viewed from the kinociliar side, the same model shows apical insertions of the SO (arrows) on each side of the kinocilium. (Scale bars, 0.5 μm in *A–D*, and *C Inset*); 1 μm in *E* and *F*.) Cal, calyx; CP, cuticular plate; KC, kinocilium; M, mitochondria.

SO Formation in Relation to Development of the Ear. Using α-2 spectrin as a marker for the SO, we performed confocal immunofluorescent (Fig. 5 *D–F*) and TEM (Fig. 5 *G–J*) studies on developing rats during the first two postnatal weeks, a period of rapid hair-cell differentiation and afferent development (21). The SO was not present at birth (postnatal day 0, P0) (Fig. 5*D*), but developed rapidly during the first week, making its first appearance at P2 (Fig. 5 *E*, *G*, and *H*), and appearing to be fully developed by P6 (Fig. 5 *F*, *I*, and *J*). Because transducer currents develop between embryonic day (E)16 and E17 in the mouse (22), and perhaps 1–2 d later in rats, the initial development of transduction does not require the SO, but it may be required for hair-cell maturation.

Discussion

Previous studies provided descriptions of the SO (7–11, 15, 16, 18) but were unable to generate a 3D view of the structure. In this study we did so using EMT. Our reconstructions show that the SO of type I hair cells has the shape of an inverted, open-ended cone (a frustum), conforming to the shape of the hair-cell neck. This cone consists of 35–40 thick filamentous bundles and an equal number of thin bundles, with an apical extension near the kinocilium, connected to the neighboring apical hair-cell membrane. In the lower, constricted neck region, thick filament bundles occasionally merge with each other. The upper ends of at least a few thick circumferential filament bundles of the SO connect to SRs and several mitochondria appear tethered to SRs and to SO bundles. The lower portions of the SO appear to insert into the plasma membrane. These associations with other elements of the cell suggest that the SO may be involved in regulation of hair-cell transduction, as well as contribute to the characteristic shape of the type I hair cell. In the type II cell, the SO has a more planar appearance and is not connected to stereocilia or the apical membrane, suggesting a predominantly structural role.

Our data provide a fresh view of the relationship between the stereociliar bundle and the cuticular plate. In most accounts, individual stereocilia have been thought to insert into the cuticular plate and terminate there. The cuticular plate is then envisioned as providing a platform that contributes to the stereocilia returning to their normal upright positions after bending (6). That SRs actually traverse the cuticular plate has been noted only occasionally in the literature (17, 23). Our data are unique in showing that the SRs reach the plasma membrane opposite the kinocilium. Stabilization of the cuticular plate itself and how it might be anchored has only been adequately explained in cochlear outer hair cells: the cuticular plate extends to the apicolateral wall of the cell (23–25), and stereocilia insert in the lateral cell membrane while still within the cuticular plate (23). This process is not the case in inner hair cells nor in vestibular hair cells (26). What provides a foundation for the cuticular plate and thus stabilizes its position? Jaeger et al. (27) showed that the cuticular plate in bullfrog hair cells was connected to the axial cytoskeleton through a well-defined bundle of microtubules. The present data show that the hair bundle and cuticular plate are even better fixed at three points on the cell membrane: the rootlets bend and extend through the cuticular plate, inserting into the plasma membrane at two points opposite the kinocilium, and the apical SO inserts into the apical cell membrane surrounding the kinocilium. These three attachments potentially form a tripod-like structure, coupling stereocilia and the kinocilium with subcuticular cytoskeletal elements, possibly affecting mechanotransduction.

The bending of SRs inside the cuticular plate is an intriguing finding. The only previous description of such bending is a single photomicrograph of a bent SR (26). There may be a molecular

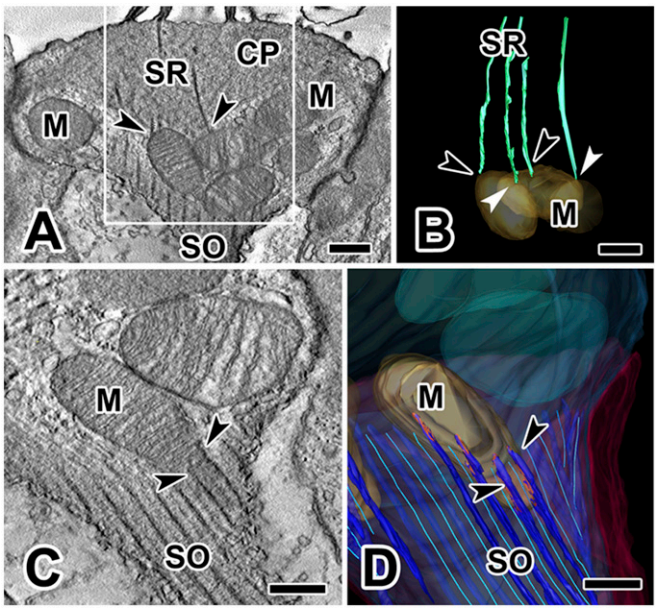

Fig. 3. Connections between subcuticular mitochondria and SRs or SO filaments. (*A*) Cell 1: SRs can terminate on subcuticular mitochondria (arrowheads); left arrowhead points to a mitochondrion that receives two distinct rootlets. (*B*) Model view of area enclosed in white box in *A* shows contacts between the distal end of several rootlets and subcuticular mitochondria. Two black arrowheads are identical to those in *A*; two white arrowheads point to additional mitochondrial-rootlet connections. (*C* and *D*) Cell 2: SO filaments are closely associated (arrowheads) with subcuticular mitochondria, as seen in a tomogram section (*C*) and in a model view (*D*) that highlights linkages (red) between the SO and subcuticular mitochondria. (Scale bars, 0.25 μm.) CP, cuticular plate; M, mitochondria.

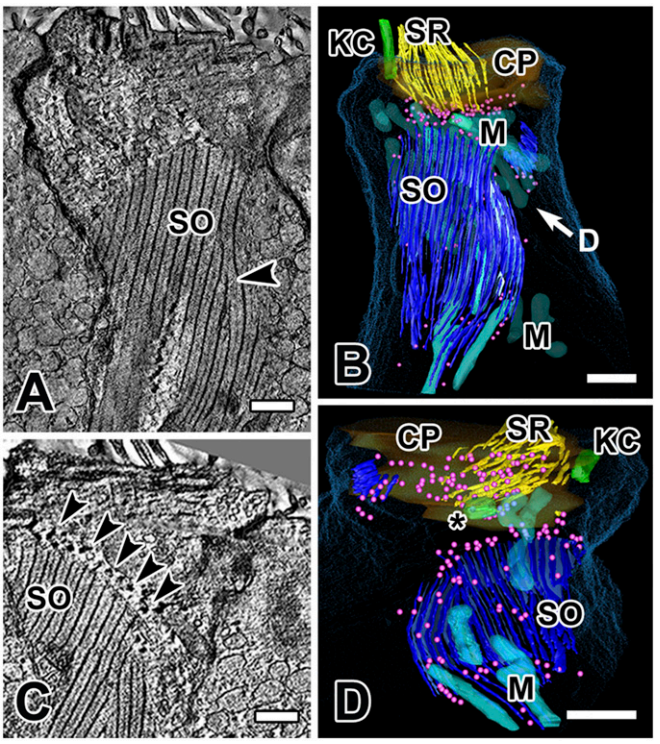

Fig. 4. The striated organelle in cell 4, an extrastriolar type II hair cell, modeled by joining nine serial tomograms (total volume thickness = 4.5 μm). (*A*) A large portion of the SO is visualized in a single plane in SLICER mode, illustrating the planar nature of the SO in type II cells. Morphing of a thick bundle into a thin one can be observed (arrowhead). (*B*) A partial 3D reconstruction of the same hair cell. "D" in *B* refers to the view in *D* (i.e., from under the cuticular plate). (*C*) In another section from the same hair cell, note the dense spherical objects (arrowheads, depicted as pink spheres in *B* and *D*) aligned with many of the thin filaments along the margins of the SO. (*D*) View from below the cuticular plate: SRs are not connected to the SO, but may be associated with the dense spherical objects (pink spheres). Most mitochondria, except for those in close association with the SO, have been removed for clarity. (Scale bars, 0.5 μm.) CP, cuticular plate; KC, kinocilium; M, mitochondria; *, centriole.

correlate for this bend. Actin is the major component of SRs (16, 23, 28). The particular angle of the bend in the SRs (110°) is similar to that produced by the actin-related proteins, Arp2/3 (actin-related protein 2/3 complex) (29–31) and coronin (32). In our material, only the longest and thickest rootlets, derived from stereocilia nearest the kinocilium and passing through the cuticular plate, exhibited this 110° angle; shorter rootlets (those that did not emerge from the cuticular plate) exhibited less acute angles.

Another prominent feature is the aggregation of large mitochondria in the subcuticular region of type I cells. Mitochondrial functional capacity is related to both overall size and internal structure (33). Such subcuticular aggregation of mitochondria with large volumes and surface areas, and "tethering" (34, 35) indicate the need for tight control of calcium homeostasis or that the SO, SRs, and other structures in the apical part of the hair cell may have high energetic requirements. Recent experiments in cochlear outer hair cells demonstrated that apical mitochondria can act to block Ca^{2+} diffusion into the hair-cell soma (36). In addition, mitochondrial crista structure has recently been related to the high metabolic rate of synapses at the calyx of Held (33). Further studies can provide structural details relevant to the functional status of these apical mitochondria (e.g., ratios of cristae to outer membrane surface area, and analysis of crista junction diameter and density).

Previous immunohistochemical studies have provided data on proteins in this part of the cell. The cuticular plate of vestibular hair cells is immunoreactive for actin, tropomyosin, and myosin (16, 37). Demêmes and Scarfone (38) demonstrated fodrin (α-2 spectrin) immunoreactivity in the SO and cuticular plate and suggested that fodrin participates in a Ca^{2+}-dependent cross-linking of actin filaments. Although we have not yet been able to confirm actin, we have confirmed by EM immunogold, Western blot, and mass spectrometry that α-2 spectrin is an integral, major component of the SO.

Physiological studies support a contractile hypothesis for something in the neck of the type I, but not type II, hair cell. K^+ depolarization induces not only reversible shape changes in type I hair cells (39–41), but also a rise in cytosolic Ca^{2+} concentration (42) that could trigger such changes. Rising Ca^{2+} levels have been suggested as a potential substrate for mechanotransduction (3), with the large SO-associated mitochondria potentially playing a role (36, 43) by promoting reuptake of Ca^{2+} after mechanotransduction. A prior study (44) has shown that in the presence of local elevated calcium levels, fodrin (α-2 spectrin) can change from a diffuse distribution within the cytoplasm to a submembranous position, or a patch. If this were also the case in hair cells, it is conceivable that the SO could change its dimensions and rigidity depending on variations in intracellular Ca^{2+} concentration (with the latter regulated, in part, by the large subcuticular mitochondria), and thus influence hair bundle or cuticular plate movements, or tilting of the cell neck. Any of these actions could alter the sensitivity of the transduction apparatus, and thus, mechanotransduction (45). Rüsch and Thurm (46) showed that hair bundles at different sites on the sensory epithelium exhibit differences in amplitude and in the time course of deflection. Our data suggest that some of these differences could be because of variations in cuticular plate size, hair-bundle size, SO shape, cross-linking, or perhaps even mitochondrial size.

Our findings suggest a dual function for the SO in type I hair cells. One structural role is as a cytoskeletal specialization

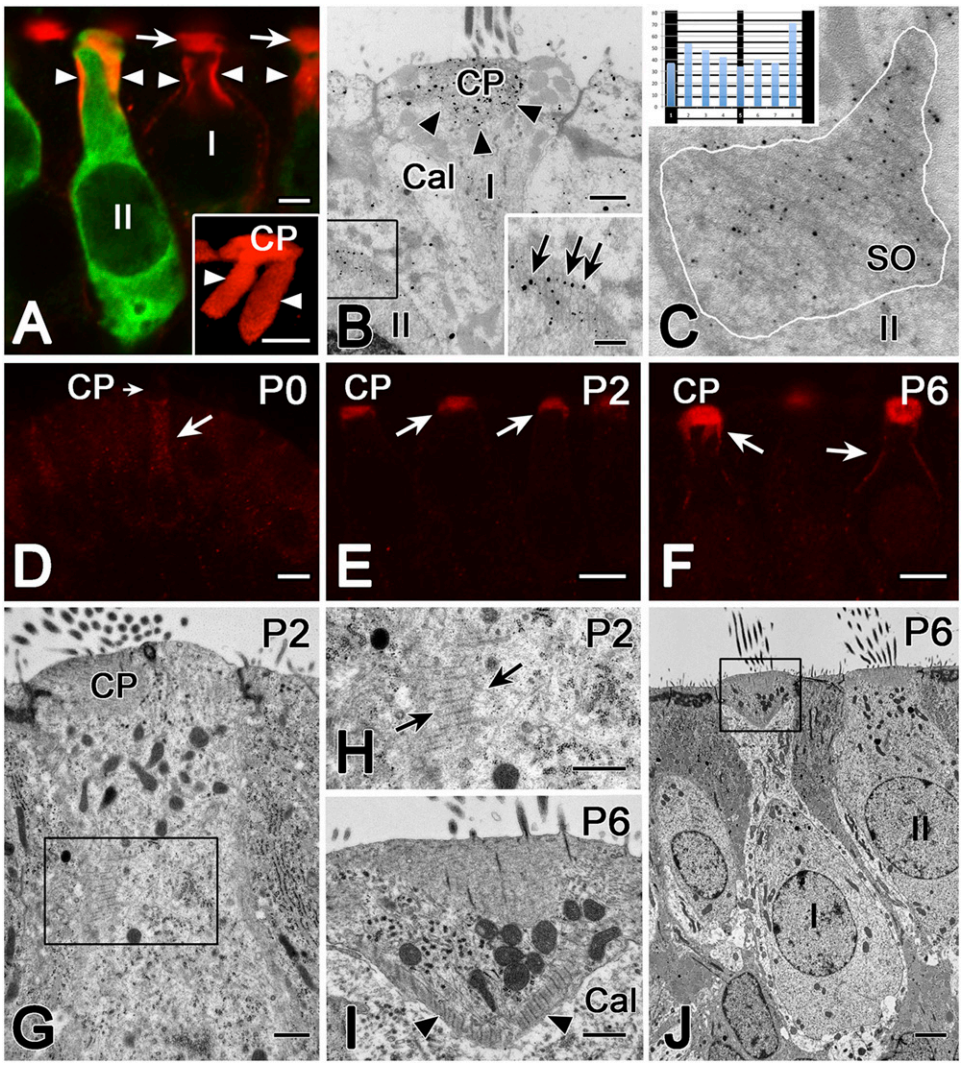

Fig. 5. The α-2 spectrin is one protein component of the SO. (*A*) Confocal microscopy shows cuticular plate (arrows) and SO (arrowheads) immunoreactivity for α-2 spectrin (red). Calretinin antibody (green) distinguishes type II (II) from type I (I) hair cells. (*Inset*) Higher magnification Volocity reconstruction of α-2 spectrin label (red) in a type II hair cell shows the SO, which appears to hang down in two large flaps (arrowheads) from the cuticular plate (CP). (Scale bars, 2 μm.) (*B*) EM immunogold with an antibody to α-2 spectrin (gold particles) localizes the protein to the cuticular plate (arrowheads) in a type I cell (I) and to the SO (black box) in a type II cell (II). (*Inset*) Higher magnification of the area enclosed within the box in *B*. Gold particles (arrows) had a tendency to be located over the cross-links between the thick and thin filament bundles. (Scale bars, 0.5 μm.) (*C*) Quantification of the α-2 spectrin EM immunogold results. In 14 SO profiles, such as this example (SO) from a type II hair cell (II), gold particles were identified within an area delineated by a white line circumscribing the SO profile. Starting with each thick filament bundle, intervals between thick bundles were divided into eight equally spaced samples running parallel to the thick bundles, and the interval into which each particle fell was determined. (*Inset*) For 363 particles, sums in the eight sample bins are illustrated, superimposed upon a schematic of the SO. A χ^2 test of homogeneity ($\chi^2 = 23.1$, $df = 7$, $P < 0.002$) indicated a preference for intervals immediately adjacent to the thick filament bundles. (*D–F*) Confocal microscopy of α-2 spectrin antibody in developing rat crista in the first postnatal week. (*D*) At birth (P0), there is no label in the cuticular plate (CP, short arrow), and only weak immunoreactivity in the upper half of the hair cell. (*E*) At P2, α-2 spectrin antibody labels the cuticular plate less intensely than at P6 (*F*), when it also labels parts of the lateral membrane in the region of the SO. (Scale bars, 5 μm.) (*G–J*) Normal TEM of developing rat hair cells. At P2 (*G* and *H*), the SO is just beginning to form in a hair cell of indeterminate type. The calyx ending, which defines type I hair cells, typically does not begin to form until P4 (21). (Scale bars in *G* and *H*, 0.5 μm.) At P6 (*I* and *J*), both the calyx (Cal) surrounding the type I cell and the SO (arrowheads) are well developed. Several stereociliar rootlets can also be observed within the cuticular plate in *I*. (Scale bars, 0.5 μm in *I* and 2 μm in *J*.)

responsible for the constricted neck characteristic of these hair cells (10, 15, 18). The architecture of the SO in type I and type II cells is one of many differences, besides $I_{K,L}$ (the outward potassium current present in type I hair cells), of a functional difference between type I and type II cells (47). Another potential structural role is to provide a tripartite foundation for the cuticular plate. Neither structural requirement is obviously present in type II hair cells, nor was a tripartite arrangement present in the one type II hair cell we reconstructed. Its columnar shape is similar to many columnar epithelial cells lacking an SO. Concerning a dynamic role, the overall architecture of the apical region in type I cells—a cluster of large mitochondria constrained between the SO and the cuticular plate, the plasma membrane and the adjacent calyx, the dense-cored vesicles—suggests that the SO is part of a larger functional complex regulating mechanotransduction or other physiological functions. Further analysis of the morphology, composition, and location, in combination with physiological studies, should shed light on its function.

Materials and Methods

Animals. Normal adult chinchillas (*Chinchilla lanigera*) were used for tomographic studies. Adult Long-Evans rats (*Rattus norvegicus*), weighing 230–330 g, were used for immunochemistry studies. For the development studies, 14 Long-Evans rat pups were studied. Two pups were killed on each day (beginning at birth, P0 to P6), one for immunofluorescent studies and the other for TEM. The Institutional Animal Care and Use Committee at the University of Illinois approved procedures involving animals.

EMT. We used serial sections of chinchilla utricular macula for conventional TEM and for IVEM. Our TEM methods were described previously (45). We analyzed a total of 41 tomograms using research facilities at the National Center for Microscopy and Imaging Research. For each reconstruction, a series of images at regular tilt increments was collected as described previously (30).

Three-Dimensional Reconstruction. Pixel sizes in our reconstructions were 2.8 nm and 1.96 nm. IMOD software (46) was used for alignment. Warped reconstructions were processed with TxBR software (47). Measurements were made with 3dmod ("Object info" feature). Stereocilia and rootlet perimeters were measured at the same distance above the cell membrane (5.6 nm). Volumes and surface areas of mitochondria below the cuticular plate and within 6 μm of the apical surface of the cell were also measured. Movies were made with Amira software (version 5.2.1, Mercury/TGS).

Antibodies. Primary antibodies were: mouse anti–α-2 spectrin (Chemicon), goat anticalretinin (Chemicon). Secondary antibodies for confocal experiments

(Chemicon) were: Alexa 488-conjugated donkey anti-goat; Alexa 594-conjugated donkey anti-mouse. Secondary antibody for EM immunogold experiments (Aurion, EM Sciences) were: gold-conjugated rabbit anti-mouse. We used calretinin antibody as a marker of hair-cell type (48).

Immunohistochemistry. Three rats were used for immunohistochemical studies and three for Western blots. Fixation, confocal microscopy, and EM immunogold procedures were identical to those described in a recent study (48), which can be consulted for details.

EM Immunogold Quantification. To test if there were a nonuniform distribution of particles, we divided SO profiles into intervals starting with each thick filament bundle, divided each interval into eight equally spaced samples parallel to the filament bundles, and determined the interval into which each particle fell. A χ^2 test of homogeneity was performed.

More detailed descriptions of EM tomography, immunogold quantification, mass spectrometry, and Western blot analysis are given in *SI Materials and Methods*.

ACKNOWLEDGMENTS. We thank Mr. Steven D. Price, Mr. John Crum, and Mr. Mason Mackey for excellent technical assistance; Dr. Larry Helseth at the Chicago Biomedical Consortium-University of Illinois at Chicago Proteomics, Metabolomics and Informatics Services Facility in the Research Resources Center (which was established in part by a grant from The Searle Funds at the Chicago Community Trust to the Chicago Biomedical Consortium) for assistance in analysis of the mass spectrometry data; and Dr. Jay M. Goldberg and the anonymous reviewers for providing critical comments on a previous version of the manuscript. This work was supported by National Institutes on Deafness and other Communication Disorders Grant DC-02521 and a grant from the American Hearing Research Foundation (to A.L.); the 2008 Tallu Rosen Grant in Auditory Science from the National Organization for Hearing Research Foundation (to A.L. and F.V.); and National Center for Recearch Resources Grant P41 RR004050 (to M.H.E.).

1. Dierkes K, Lindner B, Jülicher F (2008) Enhancement of sensitivity gain and frequency tuning by coupling of active hair bundles. *Proc Natl Acad Sci USA* 105: 18669–18674.
2. Fettiplace R, Hackney CM (2006) The sensory and motor roles of auditory hair cells. *Nat Rev Neurosci* 7:19–29.
3. Hudspeth AJ (2005) How the ear's works work: Mechanoelectrical transduction and amplification by hair cells. *C R Biol* 328:155–162.
4. DeRosier DJ, Tilney LG (1989) The structure of the cuticular plate, an in vivo actin gel. *J Cell Biol* 109:2853–2867.
5. Forge A, Wright T (2002) The molecular architecture of the inner ear. *Br Med Bull* 63: 5–24.
6. Tilney MS, et al. (1989) Preliminary biochemical characterization of the stereocilia and cuticular plate of hair cells of the chick cochlea. *J Cell Biol* 109:1711–1723.
7. Friedmann I, Cawthorne T, McLay K, Bird ES (1963) Electron microscopic observations on the human membranous labyrinth with particular reference to Méniére's Disease. *J Ultrastruct Res* 49:123–138.
8. Friedmann I, Cawthorne T, Bird ES (1965) Broad-banded striated bodies in the sensory epithelium of the human macula and in neurinoma. *Nature* 207:171–174.
9. Ross MD, Bourne C (1983) Interrelated striated elements in vestibular hair cells of the rat. *Science* 220:622–624.
10. Slepecky N, Hamernik R, Henderson D (1981) The consistent occurrence of a striated organelle (Friedmann body) in the inner hair cells of the normal chinchilla. *Acta Otolaryngol* 91:189–198.
11. Spoendlin H (1966) The organization of the cochlear receptor. *Adv Otorhinolaryngol* 13:1–227.
12. Hoshino T (1975) An electron microscopic study of the otolithic maculae of the lamprey (*Entosphenus japonicus*). *Acta Otolaryngol* 80:43–53.
13. Mørup Jørgensen J (1982) Microtubules and laminated structures in inner ear hair cells. *Acta Otolaryngol* 94:241–248.
14. Peusner KD, Lindberg NH, Mansfield PF (1988) Ultrastructural study of calycine synaptic endings of colossal vestibular fibers in the cristae ampullares of the developing chick. *Int J Dev Neurosci* 6:267–283.
15. Slepecky N, Hamernik RP, Henderson D (1980) A re-examination of a hair cell organelle in the cuticular plate region and its possible relation to active processes in the cochlea. *Hear Res* 2:413–421.
16. Slepecky N, Chamberlain SC (1985) Immunoelectron microscopic and immunofluorescent localization of cytoskeletal and muscle-like contractile proteins in inner ear sensory hair cells. *Hear Res* 20:245–260.
17. Takasaka T, Shinkawa H, Hashimoto S, Watanuki K, Kawamoto K (1983) High-voltage electron microscopic study of the inner ear. Technique and preliminary results. *Ann Otol Rhinol Laryngol Suppl* 101:1–12.
18. Sans A (1989) Ultrastructural study of striated organelles in vestibular sensory cells of human fetuses. *Anat Embryol (Berl)* 179:457–463.
19. Auer M, et al. (2008) Three-dimensional architecture of hair-bundle linkages revealed by electron-microscopic tomography. *J Assoc Res Otolaryngol* 9:215–224.
20. Lenzi D, Runyeon JW, Crum J, Ellisman MH, Roberts WM (1999) Synaptic vesicle populations in saccular hair cells reconstructed by electron tomography. *J Neurosci* 19: 119–132.
21. Rüsch A, Lysakowski A, Eatock RA (1998) Postnatal development of type I and type II hair cells in the mouse utricle: acquisition of voltage-gated conductances and differentiated morphology. *J Neurosci* 18:7487–7501.
22. Géléoc GS, Holt JR (2003) Developmental acquisition of sensory transduction in hair cells of the mouse inner ear. *Nat Neurosci* 6:1019–1020.
23. Furness DN, Mahendrasingam S, Ohashi M, Fettiplace R, Hackney CM (2008) The dimensions and composition of stereociliary rootlets in mammalian cochlear hair cells: Comparison between high- and low-frequency cells and evidence for a connection to the lateral membrane. *J Neurosci* 28:6342–6353.
24. Liberman MC, Dodds LW (1987) Acute ultrastructural changes in acoustic trauma: Serial-section reconstruction of stereocilia and cuticular plates. *Hear Res* 26:45–64.
25. Nunes FD, et al. (2006) Distinct subdomain organization and molecular composition of a tight junction with adherens junction features. *J Cell Sci* 119:4819–4827.
26. Liberman MC (1987) Chronic ultrastructural changes in acoustic trauma: Serial-section reconstruction of stereocilia and cuticular plates. *Hear Res* 26:65–88.
27. Jaeger RG, Fex J, Kachar B (1994) Structural basis for mechanical transduction in the frog vestibular sensory apparatus: II. The role of microtubules in the organization of the cuticular plate. *Hear Res* 77:207–215.
28. Tilney LG, DeRosier DJ (1986) Actin filaments, stereocilia, and hair cells of the bird cochlea. IV. How the actin filaments become organized in developing stereocilia and in the cuticular plate. *Dev Biol* 116:119–129.
29. Maiti S, Bamburg J (2004) Actin-capping and -severing proteins. *Encylopedia of Biological Chemistry*, eds Lennarz WJ, Lane MD, pp 19–26.
30. Mullins RD, Heuser JA, Pollard TD (1998) The interaction of Arp2/3 complex with actin: Nucleation, high affinity pointed end capping, and formation of branching networks of filaments. *Proc Natl Acad Sci USA* 95:6181–6186.
31. Saarikangas J, Zhao H, Lappalainen P (2010) Regulation of the actin cytoskeleton-plasma membrane interplay by phosphoinositides. *Physiol Rev* 90:259–289.
32. Cai L, Makhov AM, Schafer DA, Bear JE (2008) Coronin 1B antagonizes cortactin and remodels Arp2/3-containing actin branches in lamellipodia. *Cell* 134:828–842.
33. Perkins GA, et al. (2010) The micro-architecture of mitochondria at active zones: Electron tomography reveals novel anchoring scaffolds and cristae structured for high-rate metabolism. *J Neurosci* 30:1015–1026.
34. Boncompagni S, et al. (2009) Mitochondria are linked to calcium stores in striated muscle by developmentally regulated tethering structures. *Mol Biol Cell* 20: 1058–1067.
35. Csordás G, et al. (2010) Imaging interorganelle contacts and local calcium dynamics at the ER-mitochondrial interface. *Mol Cell* 39:121–132.
36. Beurg M, Nam JH, Chen Q, Fettiplace R (2010) Calcium balance and mechanotransduction in rat cochlear hair cells. *J Neurophysiol* 104:18–34.
37. Hasson T, et al. (1997) Unconventional myosins in inner-ear sensory epithelia. *J Cell Biol* 137:1287–1307.
38. Demêmes D, Scarfone E (1992) Fodrin immunocytochemical localization in the striated organelles of the rat vestibular hair cells. *Hear Res* 61:155–160.
39. Zenner HP (1986) Motile responses in outer hair cells. *Hear Res* 22:83–90.
40. Didier A, Decory L, Cazals Y (1990) Evidence for potassium-induced motility in type I vestibular hair cells in the guinea pig. *Hear Res* 46:171–176.
41. Tanigawa T (1997) Motility of the vestibular hair cell of the guinea pig and bull frog. *Nippon Jibiinkoka Gakkai Kaiho*, 100:264.275. Japanese.
42. Chabbert C, Devau G, Sladeczek F, Lehouelleur J, Sans A (1991) Intracellular free calcium in isolated vestibular hair cells and potassium iontophoresis. *Neuroreport* 2: 243–246.
43. Szabadkai G, Duchen MR (2008) Mitochondria: The hub of cellular Ca^{2+} signaling. *Physiology (Bethesda)* 23:84–94.
44. Perrin D, Aunis D (1985) Reorganization of alpha-fodrin induced by stimulation in secretory cells. *Nature* 315:589–592.
45. Rabbitt RD, Boyle R, Highstein SM (2010) Mechanical amplification by hair cells in the semicircular canals. *Proc Natl Acad Sci USA* 107:3864–3869.
46. Rüsch A, Thurm U (1989) Cupula displacement, hair bundle deflection, and physiological responses in the transparent semicircular canal of young eel. *Pflugers Arch* 413:533–545.
47. Rüsch A, Eatock RA (1996) A delayed rectifier conductance in type I hair cells of the mouse utricle. *J Neurophysiol* 76:995–1004.
48. Lysakowski A, et al. (2011) Molecular microdomains in a sensory terminal, the vestibular calyx ending. *J Neurosci* 31:10101–10114.